



Cite this: *Chem. Commun.*, 2017, 53, 384

Received 15th October 2016,  
Accepted 2nd December 2016

DOI: 10.1039/c6cc08318h

www.rsc.org/chemcomm

# Rh(0)/Rh(III) core-shell nanoparticles as heterogeneous catalysts for cyclic carbonate synthesis†

Younjae Jung,<sup>‡,a</sup> Taeil Shin,<sup>‡,a</sup> Kiseong Kim,<sup>a</sup> Hyeeyun Byun,<sup>a</sup> Sung June Cho,<sup>\*b</sup> Hyunwoo Kim<sup>\*a,c</sup> and Hyunjoon Song<sup>\*a,c</sup>

**Rh(0)/Rh(III) core-shell nanoparticles were prepared by surface oxidation of Rh nanoparticles with *N*-bromosuccinimide. They were employed as heterogeneous catalysts for cyclic carbonate synthesis from propylene oxide and CO<sub>2</sub>, and exhibited high activity and excellent recyclability due to Lewis acidic Rh(III) species on the shells.**

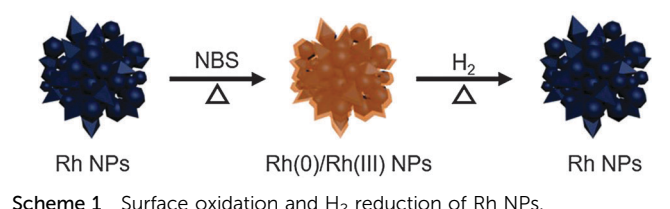
Numerous studies have been carried out in the field of homogeneous catalysis for fine chemical synthesis, due to the exact control of catalyst structures leading to high activity and selectivity of desired reactions.<sup>1–3</sup> However, the difficulties in separation from reaction products and insufficient catalyst reusability mean that heterogeneous catalysts are preferred in industry.<sup>4–8</sup> On the other hand, metal nanoparticles (NPs) not only have the advantages of heterogeneous catalysts, but also exhibit high activity and intriguing selectivity resulting from their well-defined surface facets and variable ligands bound to the surface.<sup>9–14</sup> However, metal NPs are employed in only a narrow range of organic reactions, because the oxidation states of active surface species are limited to neutral metal(0),<sup>12,15</sup> although high-valent metal complexes are widely utilized for various reactions, such as Lewis-acid catalysis and C–H functionalization.<sup>16–19</sup>

Recently, Toste and Somorjai developed new catalytic systems based on small metal clusters with the expectation of advantages for both homogeneous and heterogeneous catalysts. Upon activation with PhICl<sub>2</sub>, highly charged metal species, such as Pt(IV) and Au(III), were generated, and showed high activity in hydroalkoxylation reactions.<sup>20,21</sup> We have also reported the generation of Pd(IV) species from Pd NPs using various oxidants, which were successfully employed as Lewis-acid catalysts.<sup>22</sup> These active cationic

species were embedded on either bulk mesoporous silica or thin silica shells to ensure their stability against agglomeration.<sup>23,24</sup>

In this study, we introduce the surface oxidation of Rh NPs to provide high-valent metal species for catalytic organic reactions. Upon a simple treatment with *N*-bromosuccinimide (NBS), Rh(III) species were predominantly generated from the original Rh(0) surface, yielding Rh(0)/Rh(III) core-shell NPs, the detailed structure of which was analysed by X-ray absorption spectroscopy (XAS). Additional H<sub>2</sub> treatment of the NPs regenerated the original Rh(0) NPs without significant morphological change (Scheme 1). The activated Rh(0)/Rh(III) NPs, due to the enhanced Lewis acidity, were found to be highly active for a coupling of propylene oxide and CO<sub>2</sub> to selectively provide propylene carbonate. The cyclic carbonate synthesis is known to be catalysed by various homogeneous Lewis acid catalysts, such as Al(III), Co(III), or Zn(II).<sup>25–27</sup> To meet the demand of industrial processes, homogeneous metal species were commonly immobilized on silica, but there have been no reports thus far on the direct use of heterogeneous catalysts. The highly active Lewis acidic Rh(0)/Rh(III) catalyst can be recycled five times without loss of conversion, showing a supreme feature of heterogeneous catalysis.

The Rh NPs were prepared *via* thermal decomposition of the Rh precursor, Rh(acac)<sub>3</sub> in oleylamine.<sup>28</sup> The transmission electron microscopy (TEM) image shows that the particles have a uniform morphology of a dendritic structure (Fig. 1a) with an average overall size of 39 ± 5 nm. The X-ray photoelectron spectroscopy (Fig. 1c) spectrum at the Rh 3d level shows two major peaks at 311.9 and 307.2 eV, which are assigned to Rh(0) species. The shoulders at high binding energies originate from



Scheme 1 Surface oxidation and H<sub>2</sub> reduction of Rh NPs.

<sup>a</sup> Department of Chemistry, Korea Advanced Institute of Science and Technology (KAIST), Daejeon 34141, Republic of Korea. E-mail: hwkim@kaist.edu, hsong@kaist.ac.kr

<sup>b</sup> Department of Chemical Engineering, Chonnam National University, Gwangju 61186, Republic of Korea. E-mail: sjcho@chonnam.ac.kr

<sup>c</sup> Center for Nanomaterials and Chemical Reactions, Institute for Basic Science, Daejeon 34141, Republic of Korea

† Electronic supplementary information (ESI) available. See DOI: 10.1039/c6cc08318h

‡ These authors contributed equally to this work.

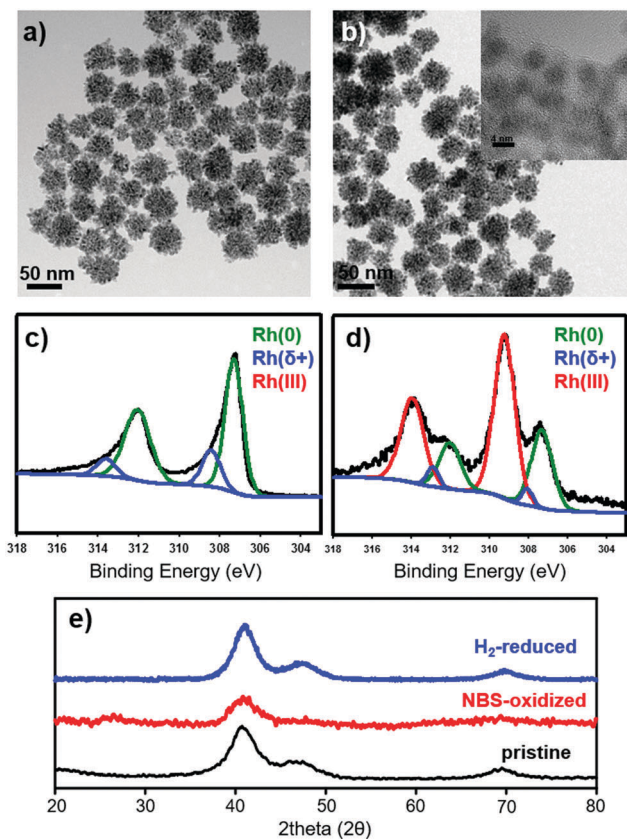


Fig. 1 (a and b) TEM and (b inset) HRTEM images and (c and d) XPS spectra at the Rh 3d level of (a and c) the pristine and (b and d) the oxidized Rh NPs. (e) XRD spectra of the pristine (black), NBS-oxidized (red), and  $H_2$ -reduced (blue) Rh NPs.

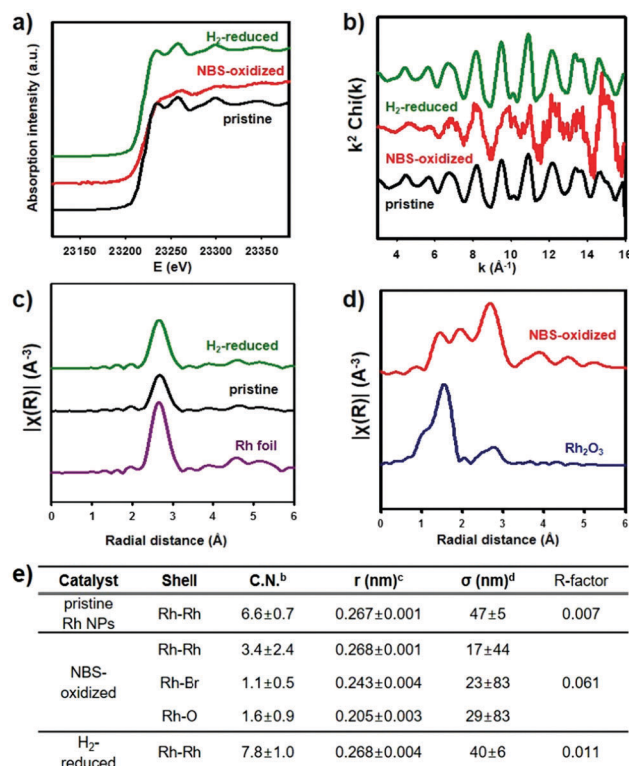
electron-deficient species (blue,  $Rh(\delta+)$ ).<sup>29</sup> The X-ray diffraction (XRD) spectrum (Fig. 1e, black) has three characteristic peaks of face-centred cubic Rh (JCPDS No. 05-0685). The average single-crystalline domain size is estimated to be 5.9 nm from the FWHM of the  $Rh(111)$  peak using the Scherrer equation.

The dendritic Rh NPs were then oxidized by treatment with 2 equiv. of oxidants, including  $PhICl_2$ , *N*-chlorosuccinimide (NCS), and *N*-bromosuccinimide (NBS) in toluene at 140 °C for 1 h. In the XPS spectra, the Rh NPs treated with NBS exhibited a distinctive increment of the shoulders at 313.9 and 309.2 eV at the Rh  $3d_{3/2}$  and  $3d_{5/2}$  levels, respectively, compared to the samples treated with other oxidants (Fig. S1, ESI†). These shoulders become major peaks after treatment with 5 equiv. of NBS (Fig. 1d and Fig. S2, ESI†), for which the de-convoluted peaks (red) are assigned to  $Rh(III)$  species. The peaks at the Br 3d level also appear at the same time (Fig. S3, ESI†). It is notable that the dendritic structure of the pristine Rh NPs hardly changes after oxidation with NBS (Fig. 1b). The high resolution TEM image (Fig. 1b inset and Fig. S4, ESI†) of the NBS-oxidized Rh NPs indicates that the single-crystalline domains with distinctive lattice fringe images are covered with amorphous layers of thicknesses of 1–2 nm, which form core-shell structures as depicted in Scheme 1. The XRD peaks are broad, meaning that the original crystallinity is significantly broken during the oxidation (red, Fig. 1e). The average

single-crystalline domain size from the  $Rh(111)$  peak is estimated to be 4.4 nm.

The reduction of the oxidized Rh NPs by  $H_2$  successfully regenerates the neutral  $Rh(0)$  surface. The XPS spectrum of the reduced NPs shows a large decrease of the  $Rh(III)$  peaks, providing a pattern similar to that of the pristine Rh NPs (Fig. S5, ESI†). The XRD spectrum also shows that the crystallinity is fully recovered by the  $H_2$  reduction (blue, Fig. 1e). These observations indicate that the structural framework of the dendritic Rh spheres is inert enough to endure the harsh conditions of oxidation and reduction, during which the surface oxidation state largely changes from  $Rh(0)$  to  $Rh(III)$  and eventually back to  $Rh(0)$  (Scheme 1).

To analyse the detailed structure and composition of the oxidized Rh NPs, XAS analysis of the samples was performed.<sup>30</sup> The Rh K-edge X-ray absorption near-edge structure (XANES) spectra of the pristine (black) and  $H_2$ -reduced (green) Rh NPs are close to that of a Rh foil reference, indicative of the zero-valence species predominant in both samples (Fig. 2a and Fig. S6, ESI†). In contrast, the NBS-oxidized NPs show a very different pattern. The  $k^2$ -weighted Rh K-edge extended X-ray absorption fine structure (EXAFS) and their Fourier-transform (FT) spectra also exhibit similar trends. As shown in Fig. 2c, the pristine and reduced Rh NPs have a strong single peak in the FT of Rh K-edge EXAFS spectra, which corresponds to single



<sup>a</sup> Inverse Fourier transformations were performed in the region of 0.100 – 0.300 nm. <sup>b</sup> Coordination number. <sup>c</sup> Bond distance. <sup>d</sup> Debye-Waller factors.

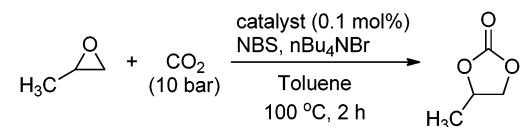
Fig. 2 (a) Rh K-edge XANES spectra, (b)  $k^2$ -weighted Rh K-edge EXAFS spectra, FT of  $k^2$ -weight Rh K-edge with (c)  $Rh(0)$  and (d)  $Rh(III)$  species, and (e) structural parameters by EXAFS refinement.

scattering by Rh–Rh atoms. On the other hand, three distinct peaks appear in the spectrum of the oxidized NPs (Fig. 2d). The structural parameters obtained by EXAFS refinement (Fig. S7, ESI†) are summarized in Fig. 2e. The peak at 2.68 Å is single scattering from Rh–Rh atoms. The peak at 2.43 Å is assigned to the scattering of Rh–Br atoms, of which the radial distance is in excellent agreement with that estimated from the major scattering peak in the FT of the Br K-edge EXAFS spectrum. The peak at 2.05 Å arises from the scattering of Rh–O atoms, nearly matching the strong peak of Rh<sub>2</sub>O<sub>3</sub> powders. These estimations are consistent with the bond distances observed in Rh salts and particles.<sup>31,32</sup> The coordination number (6.6) of the Rh–Rh atoms in the pristine Rh NPs decreases to that (3.4) in the oxidized NPs, meaning that the Rh–Rh bonds are partially broken during the oxidation. Instead, Rh–Br and Rh–O bonds are newly formed to stabilize the oxidized Rh species. Based on the metal charge (+3) from the XPS data and the coordination numbers of Rh–Br (1.1) and Rh–O (1.6) atoms from the EXAFS analysis, we suggest that the oxidation generates polymeric shells composed of  $-(\text{Rh(III)}(\text{Br})-\text{O})-$  repeating units on the surface of the Rh NPs. The presence of the pure Rh cores, proved by the XRD spectrum, indicates the formation of a Rh(0)/Rh(III) core-shell structure.<sup>33</sup> Upon the H<sub>2</sub> treatment, the Rh(III) shells are reduced to Rh(0) atoms and then the Rh–Rh bonds are recovered with neighbouring Rh atoms, leading to increase of the coordination number to 7.8. The TEM images and EXAFS analysis also confirm that the Rh NPs are inert during the oxidation and reduction processes, due to the reversible coordination of heteroatoms, Br and O, on the Rh atoms.

The zeta potential of NPs is a measure of their electrostatic stabilization, reflecting an average surface charge.<sup>34</sup> The zeta potential of the pristine Rh NPs is 23 mV, for which the positive charge may arise from oleylamine bound to the surface. The NBS-oxidized Rh NPs showed an abnormally high potential of –76 mV, which is negatively more than three times larger than that of the pristine Rh NPs. This negative potential is developed due to an electrical double layer formed around the highly charged Rh(III) species. The H<sub>2</sub> reduction returns the zeta potential back to 29 mV, similar to the potential of the pristine Rh NPs.

Rh NPs are known as excellent catalysts for various organic reactions, including hydrogenation and hydroformylation,<sup>35–37</sup> but the active catalytic species are restricted to Rh(0). On the other hand, our NBS-oxidized Rh NPs are promising Lewis acid catalysts due to the high surface charges resulting from the Rh(III) species. To verify this idea, we investigated the coupling of propylene oxide and CO<sub>2</sub>, which is commonly catalysed by homogeneous Lewis acid catalysts.<sup>25–27</sup> When propylene oxide (10 mmol) reacted with CO<sub>2</sub> (10 bar) at 100 °C for 2 h, tetra-*n*-butylammonium bromide (*n*Bu<sub>4</sub>NBr, 2.5 mol%), generally used as a co-catalyst, produced propylene carbonate only in a conversion of 21% (Table 1, entry 1). The conversion was not improved by the addition of either NBS (0.1 mol%) or Rh NPs (0.1 mol%) (Table 1, entries 2 and 3). However, the simultaneous addition of Rh NPs and NBS significantly enhanced the conversion to 83%, whereas the homogeneous Rh(I), Rh(II), and

Table 1 Propylene carbonate synthesis from propylene oxide and CO<sub>2</sub> using homogeneous and heterogeneous Rh catalysts<sup>a</sup>

				
No. <sup>a</sup>	Catalyst	NBS (mol%)	<i>n</i> Bu <sub>4</sub> NBr (mol%)	Conv. <sup>b</sup> (%)
1	—	—	2.5	21
2	—	0.1	2.5	22
3	Rh NPs	—	2.5	22
4	Rh NPs	0.1	2.5	83
5	Rh(acac)(CO) <sub>2</sub>	—	2.5	49
6	Rh <sub>2</sub> (OAc) <sub>4</sub>	—	2.5	28
7	Rh(acac) <sub>3</sub>	—	2.5	26
8	Rh NPs	0.5	2.5	> 99
9	Rh NPs	0.5	—	0

<sup>a</sup> Conditions: propylene oxide (10 mmol) and toluene (0.2 mL) in a stainless steel pressure reactor without exclusion of air or moisture.  
<sup>b</sup> Determined by <sup>1</sup>H NMR spectra.

Rh(III) catalysts showed low to moderate conversions (26–49%) (Table 1, entries 4–7). In addition, the use of NCS or PhICl<sub>2</sub> instead of NBS gave the products in 44% or 28% yields, respectively (Table S1, ESI†). These results imply that the heterogeneous Rh(III) species on Rh(0)/Rh(III) core-shell NPs actually behave as a highly efficient Lewis acid catalyst. The highest conversion was achieved when the NBS concentration was increased to 0.5 mol% in the presence of *n*Bu<sub>4</sub>NBr (Table 1, entry 8). The product could not be obtained under the conditions without the addition of *n*Bu<sub>4</sub>NBr (Table 1, entry 9). The crucial role of the co-catalyst is in agreement with the proposed reaction mechanism that the activated propylene oxide bound to Lewis acidic Rh(0)/Rh(III) is attacked by a bromide ion, and CO<sub>2</sub> is then inserted to form propylene carbonate while releasing the catalyst and bromide ion.<sup>25,26</sup>

To verify these reactions *via* a heterogeneous catalytic pathway, filtration and mercury poisoning tests were conducted.<sup>38</sup> After the reaction under the conditions in entry 8, the reaction mixture was filtered, and the filtrate was analysed by ICP-OES (inductively coupled plasma-optical emission spectrometry). No signals were detected above the detection limit (<0.01 ppm) of the measurement. The reactants, NBS, and co-catalyst were then added to the filtrate and the reaction was carried out under the conditions in entry 8 in the absence of the Rh catalyst. As a result, propylene carbonate was produced in a 20% conversion, consistent with that in entry 2. The filtered catalyst particles maintained their original morphology (Fig. S8, ESI†). For the mercury poisoning test, a drop of mercury added to the reaction mixture significantly decreased the conversion from >99% to 26% under conditions identical to those in entry 8 (Fig. S9, ESI†). These control experiments indicate that the propylene carbonate synthesis mainly occurred on the heterogeneous catalytic species of the Rh NPs.

In general, the heterogeneous catalysts exhibit superior recyclability to their homogeneous counterparts. After the reaction, the Rh(0)/Rh(III) catalysts were recycled five more times under



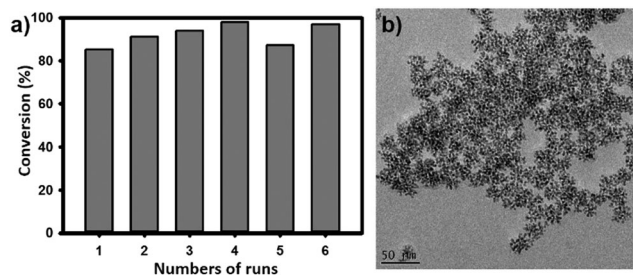


Fig. 3 (a) Recycling Rh catalysts under the conditions of entry 8 in Table 1. (b) TEM image of Rh NPs after recycling five times.

the conditions in entry 8. The reaction conversion varied within the narrow range of 85–99% during the recycling experiments (Fig. 3a). After recycling, there was no change in the morphology of the catalyst from the original dendritic structure (Fig. 3b). This high stability may result from the existence of a robust Rh(0) framework at the cores in the form of Rh(0)/Rh(III) core-shell NPs.

In conclusion, Rh(0)/Rh(III) core-shell NPs were generated by surface oxidation with NBS, and were accurately characterized by multiple X-ray spectroscopic techniques. The catalyst exhibited a quantitative yield for propylene carbonate synthesis from propylene oxide and CO<sub>2</sub>, due to the high Lewis acidity of the Rh(III) species on the shells. The reactions proceeded through a heterogeneous catalytic pathway, and thus were successfully recycled five times without damaging the catalyst morphology. The heterogeneous Rh(III) species are also expected to behave as efficient catalysts for various reactions. The similar surface oxidation of metal NPs would open a wide range of catalytic organic transformations using heterogeneous catalysts of high activity with excellent separation and recycling abilities.

This work was supported by the Saudi Aramco-KAIST CO<sub>2</sub> Management Center and IBS-R004-D1. Y. J. and H. S. thank the National Research Foundation of Korea (NRF) funded by the Korea Government (MSIP) for the support (NRF-2015R1A2A2A01004196). S. J. C. acknowledges the Korea CCS R&D Center (KCRC) grant funded by the Korean Ministry of Science, ICT & Future Planning (NRF-2014M1A8A1049254). The authors thank the Pohang Accelerator Laboratory (PAL) for beamline use. EXAFS experiments at PLS were supported by MSIP and POSTECH.

## Notes and references

- 1 J. G. de Vries, *Fine Chemical Synthesis – Homogeneous*, in *Encyclopedia of Catalysis*, John Wiley & Sons, 2002.
- 2 A. Behr and P. Neubert, *Applied Homogeneous Catalysis*, Wiley VCH, 2012.

- 3 A. Zapf and M. Beller, *Top. Catal.*, 2002, **19**, 101.
- 4 D. J. Cole-Hamilton, *Science*, 2003, **299**, 1702.
- 5 G. V. Smith and F. Notheisz, *Heterogeneous catalysis in organic chemistry*, Academic Press, San Diego, CA, 1999.
- 6 G. A. Somorjai, *Introduction to surface chemistry and catalysis*, John Wiley & Sons, New York, 1994.
- 7 A. T. Bell, *Science*, 2003, **299**, 1688.
- 8 R. A. Sheldon and H. van Bekkum, *Fine Chemicals through Heterogeneous Catalysis*, Wiley-VCH, Weinheim, 2001.
- 9 *Nanoparticles and Catalysis*, ed. D. Astruc, Wiley VCH, 2007.
- 10 G. A. Somorjai, F. Tao and J. Y. Park, *Top. Catal.*, 2008, **47**, 1.
- 11 F. Zaera, *Chem. Soc. Rev.*, 2013, **42**, 2746.
- 12 L. L. Chng, N. Erathodiyil and J. Y. Ying, *Acc. Chem. Res.*, 2013, **46**, 1825.
- 13 Y. Xia, H. Yang and C. T. Campbell, *Acc. Chem. Res.*, 2013, **46**, 1671.
- 14 T. Yauskawa, H. Miyamura and S. Kobayashi, *Chem. Soc. Rev.*, 2014, **43**, 1450.
- 15 M. J. Climent, A. Corma and S. Iborra, *Chem. Rev.*, 2011, **111**, 1072.
- 16 J. F. Hartwig, *Organotransition Metal Chemistry: From Bonding to Catalysis*, University Science Books, 2009.
- 17 P. Sehnal, R. J. K. Taylor and I. J. S. Fairlamb, *Chem. Rev.*, 2010, **110**, 824.
- 18 A. J. Hickman and M. S. Sanford, *Nature*, 2012, **484**, 177.
- 19 S. R. Neufeldt and M. S. Sanford, *Acc. Chem. Res.*, 2012, **45**, 936.
- 20 C. A. Witham, W. Huang, C.-K. Tsung, J. N. Kuhn, G. A. Somorjai and F. D. Toste, *Nat. Chem.*, 2010, **2**, 36.
- 21 E. Gross, J. H.-C. Liu, F. D. Toste and G. A. Somorjai, *Nat. Chem.*, 2012, **4**, 947.
- 22 M. Kim, S. Lee, K. Kim, D. Shin, H. Kim and H. Song, *Chem. Commun.*, 2014, **50**, 14938.
- 23 S. H. Joo, J. Y. Park, C.-K. Tsung, Y. Yamada, P. Yang and G. A. Somorjai, *Nat. Mater.*, 2009, **8**, 126.
- 24 J. C. Park and H. Song, *Nano Res.*, 2011, **4**, 33.
- 25 M. North, R. Pasquale and C. Young, *Green Chem.*, 2010, **12**, 1514.
- 26 X.-B. Lu and D. J. Darensbourg, *Chem. Soc. Rev.*, 2012, **41**, 1462.
- 27 Y. Yang, Y. Hayashi, Y. Fujii, T. Nagano, Y. Kita, T. Ohshima, J. Okuda and K. Mashima, *Catal. Sci. Technol.*, 2012, **2**, 509.
- 28 Y. Feng, X. Ma, L. Han, Z. Peng and J. Yang, *Nanoscale*, 2014, **6**, 6173.
- 29 C. Fontaine-Gautrelet, J.-M. Krafft, G. Djega-Mariadassou and C. Thomas, *J. Catal.*, 2007, **247**, 34.
- 30 Y. Li, J. H.-C. Liu, C. A. Witham, W. Huang, M. A. Marcus, S. C. Fakra, P. Alayoglu, Z. Zhu, C. M. Thompson, A. Arjun, K. Lee, E. Gross, F. D. Toste and G. A. Somorjai, *J. Am. Chem. Soc.*, 2011, **133**, 13527.
- 31 J. Reed and P. Eisenberger, *Acta Crystallogr., Sect. B: Struct. Crystallogr. Cryst. Chem.*, 1978, **34**, 344.
- 32 M. E. Strayer, J. M. Binz, M. Tanase, S. M. K. Shahri, R. Sharma, R. M. Rioux and T. E. Mallouk, *J. Am. Chem. Soc.*, 2014, **136**, 5687.
- 33 J.-I. Park, M. G. Kim, Y.-w. Jun, J. S. Lee, W.-R. Lee and J. Cheon, *J. Am. Chem. Soc.*, 2004, **126**, 9072.
- 34 N. Yan, Y. Yuan and P. J. Dyson, *Chem. Commun.*, 2011, **47**, 2529.
- 35 M. J. Jacinto, P. K. Kiyohara, S. H. Masunaga, R. F. Jardim and L. M. Rossi, *Appl. Catal., A*, 2008, **338**, 52.
- 36 K. H. Park, K. Jang, H. J. Kim and S. U. Son, *Angew. Chem., Int. Ed.*, 2007, **46**, 1152.
- 37 A. J. Bruss, M. A. Gelesky, G. Machado and J. Dupont, *J. Mol. Catal. A: Chem.*, 2006, **252**, 212.
- 38 N. T. S. Phan, M. Van Der Sluys and C. W. Jones, *Adv. Synth. Catal.*, 2006, **348**, 609.